Undulatory Locomotion of Magnetic Multilink Nanoswimmers

Journal Article

Author(s):
Jang, Bumjin; Gutmann, Emiliya; Stucki, Nicolai; Seitz, Benedikt F.; Wendel-Garcia, Pedro D.; Newton, Taylor H.; Pokki, Juho; Ergeneman, Olgaç; Pané, Salvador; Or, Yizhar; Nelson, Bradley J.

Undulatory locomotion of magnetic multi-link nanoswimmers

Bumjin Jang,[†] Emiliya Gutman,[‡] Nicolai Stucki,[†] Benedikt F. Seitz,[†] Pedro D. Wendel-García,[†] Taylor Newton,[†] Juho Pokki,[†] Olgaç Ergeneman,[†] Salvador Pané,[$,†] Yizhar Or,[‡] and Bradley J. Nelson*[,†]

[†]Institute of Robotics and Intelligent Systems, ETH Zurich, Zurich, CH-8092, Switzerland

[‡]Faculty of Mechanical Engineering, Technion – Israel Institute of Technology, Israel

ABSTRACT: Micro- and nanorobots operating in low Reynolds number fluid environments require specialized swimming strategies for efficient locomotion. Prior research has focused on designs mimicking the rotary corkscrew motion of bacterial flagella or the planar beating motion of eukaryotic flagella. These biologically inspired designs are typically of uniform construction along their flagellar axis. This work demonstrates for the first time planar undulations of composite multi-link nanowire-based chains (diameter 200 nm) induced by a planar-oscillating magnetic field. Those chains comprise an elastic eukaryote-like polypyrrole tail and rigid magnetic nickel links connected by flexible polymer bilayer hinges. The multi-link design exhibits high swimming efficiency. Furthermore, the manufacturing process enables tuning the geometrical and material properties to specific applications.

KEYWORDS: 1-, 2- and 3-link nanoswimmers, undulatory locomotion, planar oscillating magnetic field, nanowires

Recent advances in micro- and nanofabrication techniques have driven a surge of interest in the development of micro- and nanoscale robotic systems for medical applications.[1-5] Small robotic systems promise to reduce the invasiveness of a variety of medical procedures, resulting in shorter recovery times, lowered risk of complications, decreased pain, and enhanced treatment specificity.[6] However, in order to be effective, these systems must be capable of navigating the biological fluid environments found within the body. This task is complicated by the fact that as length scale decreases relative to fluid viscosity, viscous forces begin to dominate inertial forces, producing a number of counterintuitive physical effects.[7] The ratio of inertial to viscous forces is termed Reynolds number, and fluid environments dominated by viscous forces are said to have low Reynolds number. In his widely cited 1977 paper "Life at Low Reynolds Number", Edward Purcell first presented the "scallop theorem", which states that at low Reynolds number, reciprocal motion (i.e. motion that is symmetric under time reversal) does not result in net displacement.[8] The implication is that any successful micro- or nanorobotic swimmer must employ non-reciprocal (non time-symmetric) motion to achieve net displacement. To this end, multiple strategies have been explored to date, many inspired by propulsion techniques observed in nature.[9-13] As an example, Qiu, T. *et al*. have recently demonstrated propulsion of a scallop microswimmer (~700 μm) in reciprocal motion at low Reynolds number. The strategy to break a time-reversible motion was achieved by manipulating the microswimmer in a non-Newtonian fluid whose effective viscosity changes with the fluidic velocity and shear rate.[14] Nevertheless, Purcell in his paper[8] stated that in a viscous Newtonian fluid, the simplest structure capable of non-reciprocal motion at low Reynolds number is a fore-aft-symmetric linkage, with three links separated by two hinges. For the investigation of Purcell's 3-link swimmer, various theoretical models have been considered.[15-17] However, these models only consider swimmers whose joint

angles are directly controlled, while other work[18] considers controlled actuation by internal torques applied at the joints, rather than external actuation.

In this work, the planar undulation of three-link nanoswimmers under an external oscillating magnetic field has been demonstrated for the first time. The nanoswimmers consist of one polymeric and two magnetic metallic nanowire (NW) links which are connected by hinges (Figure 1a). For comparison, 1- and 2-link nanoswimmers were fabricated, and their corresponding swimming behaviour was analysed. The entire nanowire-based chains were produced adapting a sophisticated manufacturing process by Ozin and co-workers, which combines multi-step electrodeposition, layer-by-layer deposition and selective etching.[19] Detailed information regarding the experimental procedures can be found in the supporting information. This fabrication strategy enables the construction of flexible structures without directly contacting the metal segments. The hinge length can be tuned to minimize magnetic dipolar interactions and to adjust the flexibility of the chain. This manufacturing approach also offers high versatility in terms of material selection. For instance, a distinguishing aspect of our design is the use of polypyrrole (PPy), a conductive polymer, to construct a long non-magnetic link (hereafter referred to as the "tail"). PPy's elasticity allows the tail to flex during each stroke, thereby breaking the time-reversibility of the motion. The remaining two links are ferromagnetic nickel rods. These links are connected by short elastic polymeric cylinders composed of concentric layers of polyallylamine chloride (PAH) and polystyrene sulfonate (PSS). Since these polymeric cylinders have a length of 1.5 μm with a thickness of several nanometers[20], they can be effectively regarded as flexible hinges. To isolate the effects of the number of links on swimming performance, we kept the overall length of the swimmers fixed at roughly 15.5 μm. SEM and optical images of 1-, 2- and 3-link nanoswimmers are shown in Fig. 1b and c. For a 1-

link nanoswimmer, the Ni/Au head segment was visually distinguishable from the PPy tail in the optical microscope, as metals possess higher reflectivity than polymers. For the 2- and 3-link swimmers, the hinges appeared visually as empty spaces between the links since the thickness of the PAH/PSS bilayers (on the order of several nm) allowed significant light transmission through the hinges.

The nanoswimmers were actuated through the application of a planar oscillating magnetic field (Fig. 1d), which was generated using two sets of coplanar, opposing electromagnetic coil pairs situated at a ninety degree offset. In order to create an oscillating planar field, we superposed two sinusoidal oscillating field component functions as given by the equations $(B_x = B_A \cos(\theta \cdot \sin(2\pi ft))$, $B_y = B_A \sin(\theta \cdot \sin(2\pi ft))$ where B_A, θ and f are the field strength, oscillation angle (the angular sweep of the magnetic field is $2\theta)$ and frequency, respectively. Figure 2a shows the dynamic motion of a 1-link swimmer via an external field. Notably, the swimmer's magnetic Ni head continuously aligns with the orientation of the input field due to the exerted torque (τ_m), while the flexible PPy tail exhibits an undulating motion. We define the smallest radius of curvature (SROC) as the smallest radius of oscillating circle fitted to the body of the swimmer over the course of the image sequence. The SROC provides information regarding the degree of structural deformation during motion. For a typical 1-link swimmer, the SROC was found to be on the order of 36.53 ± 0.03 μm. The time-dependent deformation of the entire swimmer over its stroke cycle was characterized through the use of a structural trajectory, overlaid on the last image of the sequence in Fig. 2a. From this trajectory, we found that the planar motion of a 1-link swimmer has a pivot point close to the center of the swimmer's long axis. With respect to this pivot point, the maximal angle distributions for the fore (FMAD) and aft (AMAD) portions of the swimmer were measured to be 49.71° and 35.86°, respectively. The display pattern in

figure 2 b in which the centerlines of the swimmer in each frame are presented over time clearly shows a tendency towards undulation. This is qualitatively similar to the motion described by Purcell for a "flexible oar" style swimmer[8] whose non-time reversibility is achieved by the significant changes of bending curvature during each stroke of the flexible tail[21]. According to Lagomarsino et al., this type of undulation occurs at low sperm number where bending forces dominate viscous forces.[22] The sperm number characterizes the relative importance of viscous to bending forces on the swimmer.[9] When actuated, 1-link swimmers pivot almost as a rigid rod, which means that elastic forces are dominating.

Regarding the swimming dynamics of 2-link swimmers, we did not observe a significant difference when compared to their 1-link counterparts, except for changes in the SROC, FMAD and AMAD values (Figure 2c). Interestingly, compared to the 1-link swimmers, 2-link swimmers show a decreased SROC (14.02 ± 0.07 μm). This indicates that the structural deformation of 2-link swimmers is larger than that of 1-link swimmers, probably due to the increased mobility afforded by the presence of a hinge. The increased FMAD (64.39°) and decreased AMAD (26.35°) confirm this assumption. In Fig. 2d, we again observe the undulation as in the case of the 1-link swimmers.

Figure 2e captures the dynamics of 3-link swimmers. Similar to the 1- and 2-link swimmers, bending motion in the PPy tail was also observed for the 3-link swimmers during actuation. However unlike for 1- and 2-link swimmers, a distinct S-like motion emerges due to a time-dependent difference in orientation between the two Ni segments under the influence of the applied field. The degree of structural deformation during this S-like motion was found from decoupled SROC values for the head segment (7.21 ± 0.03 μm) and the tail segment (14.69 ± 0.08 μm). To more closely examine this phenomenon, a structural trajectory was overlaid on the

last image of the sequence in figure 2e. We observed a reduction in the FMAD (56.33°) and AMAD (19.39°) when compared with the 2-link swimmers (64.39° and 26.35°, respectively). The wave pattern visible in figure 2f has the interesting feature of a traveling wave propagating along the longitudinal axis of the swimmer. Theoretical results obtained by Lagomarsino et al. confirm that a traveling wave tends to appear in the motion of a driven filament with relatively high sperm number (high viscous to bending force ratio).[22] This feature is one of the possible ways to escape the time reciprocal motions that plague low Reynolds number systems. Experimentally, Dreyfus et al. made a similar observation in the study of a microswimmer comprising a filament-like chain of paramagnetic micro-beads connected by DNA.[9] In our study, simply adding a second hinge was sufficient to establish a traveling wave.

The swimming characteristics of 1-, 2- and 3-link swimmers were further characterized by measuring the average speed while varying the frequency f and maximum angular sweep 2θ of the applied field (Figure 3). Regardless of the swimmer type, we observed resonance-like behaviours where the speed is maximized at an optimal frequency. For too high frequencies, the swimmer's response times are too slow, its undulation amplitude decays, and, subsequently, the speed vanishes. This phenomenon of resonance frequency was observed in previous experimental work[9], and also corroborates the theoretical analysis in Gutman and Or[23].

A close look at the speed plot for 1-link swimmers in figure 3a suggests that the maximum average speed is 6.61 μm/s (0.43 body lengths/second) at a frequency of 10 Hz and a maximum angular sweep of 180 °. The maximum speed of our 1-link device is very close to that of the MagnetoSperm, a similar microswimmer detailed in a recent publication by Kahlil et al.[24] The motion of our nanoswimmer operating at maximum speed is shown in Fig. 4a (See SI Movie S4).

Figure 3b is a plot of average measured speed for 2-link swimmers. We observed an overall increase in speed for 2-links as compared to 1-link. We speculate that this is a result of the additional degree of freedom provided by the hinge as discussed previously. This additional degree of freedom results in a greater angular sweep during actuation and, therefore, more effective swimming. Figure 4b shows a time-lapse image sequence of a 2-link swimmer during actuation. The maximum speed in this case was 10.92 μm/s (0.70 body lengths/second) at a frequency of 15 Hz and a maximum angular sweep of 160 ° (see SI Movie S5).

Finally, the average speed of 3-link swimmers was measured in figure 3c. The maximum speed was 14.44 μm/s (0.93 body/sec) at a frequency of 20 Hz and a maximum angular sweep of 180 °. Figure 4c presents its propulsion at this maximum speed (see SI Movie S6). In spite of the decreased magnetic volume of the Ni segments compared to the 1- and 2-link swimmers, our 3-link swimmers possessed a higher maximal speed. We therefore inferred that the clear S-like motion exhibited by the 3-link swimmers results in greater swimming efficiency than the flexible oar pattern characteristic of 1-link swimmers.

We also plotted the net displacement per period X= V/f, which is the swimming speed V divided by frequency f, as a function of f for the 1, 2 and 3-linked swimmers, respectively (Fig. 3d, e, f.). From this, it can be seen that in most of the cases there is an optimal frequency at which X is maximized, which is smaller than the optimal frequency for maximal speed. This finding is in agreement with the analysis of the theoretical model in Gutman and Or.[23]

In conclusion, 1-, 2- and 3-link magnetic nanoswimmers have been successfully fabricated and their motion behaviour has been analysed. Analysis of the dynamics of the 1- and 2-link swimmers indicates that the observed swimming behaviour is a result of an undulation motion that mainly occurs along their flexible tails. The changes in SROC, FMAD and AMAD values

can be related to the increased speed of the 2-link swimmers as compared to the 1-link swimmers, implying that the increased freedom of the tail through the introduction a hinge is important for optimal swimming. Furthermore, an S-like motion appears for swimmers with 3-links, coupled with the emergence of a traveling wave along the length of the structure. Additionally, all swimmer types studied (1-, 2- and 3-links) were subject to a resonance-like behaviour at an optimal frequency for a given field strength. The maximum speed measured for the 1-, 2- and 3-link nanoswimmers were 0.43, 0.70 and 0.93 body–lengths s^{-1}, respectively.

ASSOCIATED CONTENT

Supporting Information.

Experimental procedures, movies about dynamic motions and propulsions at the maximum speeds of 1,2 and 3-link nanoswimmers. This material is available free of charge via the Internet at http://pubs.acs.org.

AUTHOR INFORMATION

Corresponding Authors

E-mail: * bnelson@ethz.ch, $ vidalp@ethz.ch

Author Contributions

B.J.N. and S.P. initiated the project. S.P. designed the fabrication experiments. B.J. fabricated the magnetic nanoswimmers and analyzed their motion. N.S. and B.F.S. optimized the fabrication. P.D.W.G. developed the code to extract the velocities of the swimmers. J.P. and O.E designed and provided the experimental magnetic setup for manipulation. B.J., E.G and Y.O. performed

the analysis of the swimmers and provided theoretical discussion. B.J., T.N, O.E., S.P., Y.O. and B.J.N. co-wrote the manuscript. O.E., S.P., Y.O. and B.J.N. supervised the work and gave critical input. All authors contributed to discussions.

Notes

The authors declare no competing financial interests.

REFERENCES

(1) Mhanna, R.; Qiu, F.; Zhang, L.; Ding, Y.; Sugihara, K.; Zenobi-Wong, M.; Nelson, B. J. *Small* **2014,** 10, 1953.

(2) Tottori, S.; Zhang, L.; Qiu, F.; Krawczyk, K. K.; Franco-Obregon, A.; Nelson, B. J. *Adv. Mater.* **2012,** 24, 811.

(3) Kim, S.; Qiu, F.; Kim, S.; Ghanbari, A.; Moon, C.; Zhang, L.; Nelson, B. J.; Choi, H. *Adv. Mater.* **2013,** 25, 5863.

(4) Freitas, R. A., Jr. *Int. J. Surg.* **2005,** 3, 243.

(5) Ishiyama, K.; Sendoh, M.; Arai, K. I. *J. Magn. Magn. Mater.* **2002,** 242–245, Part 1, 41.

(6) Nelson, B. J.; Kaliakatsos, I. K.; Abbott, J. J. *Annu. Rev. Biomed. Eng.* **2010,** 12, 55.

(7) Taylor, G. *Proc. R. Soc. London, Ser. A* **1951,** 209, 447.

(8) Purcell, E. M. *Am. J. Phys.* **1977,** 45, 3.

(9) Dreyfus, R.; Baudry, J.; Roper, M. L.; Fermigier, M.; Stone, H. A.; Bibette, J. *Nature* **2005,** 437, 862.

(10) Zhang, L.; Abbott, J. J.; Dong, L.; Kratochvil, B. E.; Bell, D.; Nelson, B. J. *Appl. Phys. Lett.* **2009,** 94, 064107.

(11) Tierno, P.; Golestanian, R.; Pagonabarraga, I.; Sagués, F. *Phys. Rev. Lett.* **2008,** 101.

(12) Paxton, W. F.; Kistler, K. C.; Olmeda, C. C.; Sen, A.; St. Angelo, S. K.; Cao, Y.; Mallouk, T. E.; Lammert, P. E.; Crespi, V. H. *J. Am. Chem. Soc.* **2004,** 126, 13424.

(13) Gao, W.; Sattayasamitsathit, S.; Manesh, K. M.; Weihs, D.; Wang, J. *J. Am. Chem. Soc.* **2010,** 132, 14403.

(14) Qiu, T.; Lee, T. C.; Mark, A. G.; Morozov, K. I.; Munster, R.; Mierka, O.; Turek, S.; Leshansky, A. M.; Fischer, P. *Nat. Commun.* **2014,** 5, 5119.

(15) Becker, L. E.; Koehler, S. A.; Stone, H. A. *J. Fluid Mech.* **2003,** 490, 15.

(16) Tam, D.; Hosoi, A. E. *Phys. Rev. Lett.* **2007,** 98.

(17) Passov, E.; Or, Y. *Eur. Phys. J. E Soft Matter* **2012,** 35, 78.

(18) Or, Y. *Phys. Rev. Lett.* **2012,** 108.

(19) Mirkovic, T.; Foo, M. L.; Arsenault, A. C.; Fournier-Bidoz, S.; Zacharia, N. S.; Ozin, G. A. *Nat. Nanotechnol.* **2007,** 2, 565.

(20) Deng, C.; Dong, W.-F.; Adalsteinsson, T.; Ferri, J. K.; Sukhorukov, G. B.; Möhwald, H. *Soft Matter* **2007,** 3, 1293.

(21) Namdeo, S.; Khaderi, S. N.; Onck, P. R. *Phys. Rev. E* **2013,** 88.

(22) Lagomarsino, M. C.; Capuani, F.; Lowe, C. P. *J. Theor. Biol.* **2003,** 224, 215.

(23) Gutman, E.; Or, Y. *Phys. Rev. E* **2014,** 90.

(24) Khalil, I. S. M.; Dijkslag, H. C.; Abelmann, L.; Misra, S. *Appl. Phys. Lett.* **2014,** 104, 223701.
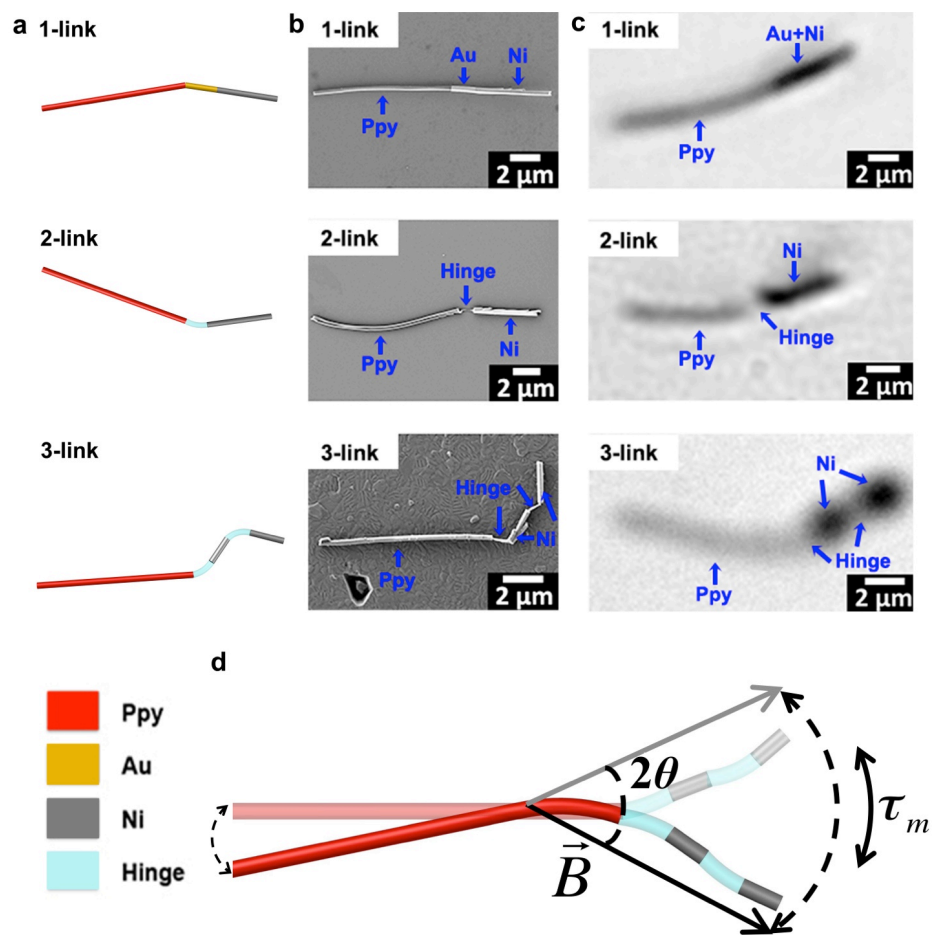
Figure 1. The characterization of 1-, 2- and 3-link swimmers and a schematic of manipulation. (a) Schematic of an 1-, 2- and 3-link swimmers. The overall length of each swimmer in approximately ≈ 15.5 μm. (b) The SEM images of 1-, 2- and 3-link of swimmers. Top: a 1-linked swimmer made of Ni (≈ 5 μm) – Au (≈ 1.5 μm) – PPy (≈ 9 μm). Middle: a 2-linked swimmer made of Ni (≈ 5 μm) - PAH/PSS (≈ 1.5 μm) – PPy (≈ 9 μm). Bottom: a 3-linked swimmer Ni (≈ 1.75 μm) - PAH/PSS (≈ 1.5 μm) – Ni (≈ 1.75 μm) - PAH/PSS (≈ 1.5 μm) – PPy (≈ 9 μm). (c) The optical images of 1-, 2- and 3-link swimmers; images correspond to the SEM images of

(b). (d) Schematic of our 3-link nanoswimmer with undulation motion, subjected to a magnetic field oscillation (2θ = angular sweep of the magnetic field, $\vec{B}$ = magnetic field and τ_m = magnetic torque).
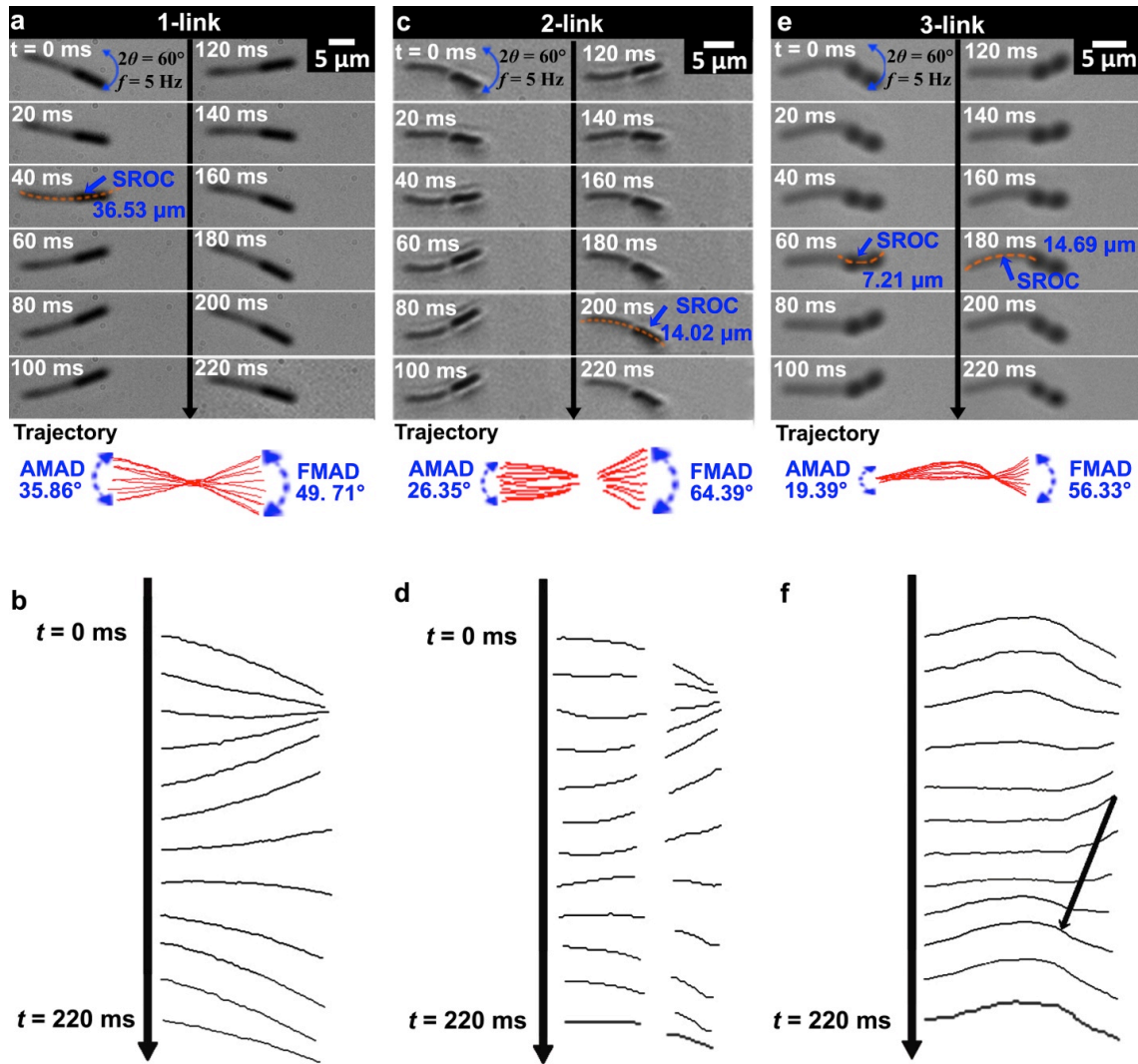

Figure 2. The characteristics of the dynamic motion of 1-, 2- and 3-link swimmers. (a),(c),(e) Image sequences of 1-, 2- and 3-link swimmers. (b),(d),(f) Display patterns of 1-, 2- and 3-link swimmers; the arrow indicates a propagation of the a bending wave. The swimmers were actuated with a magnetic field with a strength of 8.4 mT, a frequency of 5 Hz, and a maximum

angular sweep of $2\theta = 60°$. The images were acquired at 50 Hz. Swimmer structure trajectories were generated with superposing skeletonized images. *Full movies are enclosed in the supporting information (SI Movie S1, 2, 3).
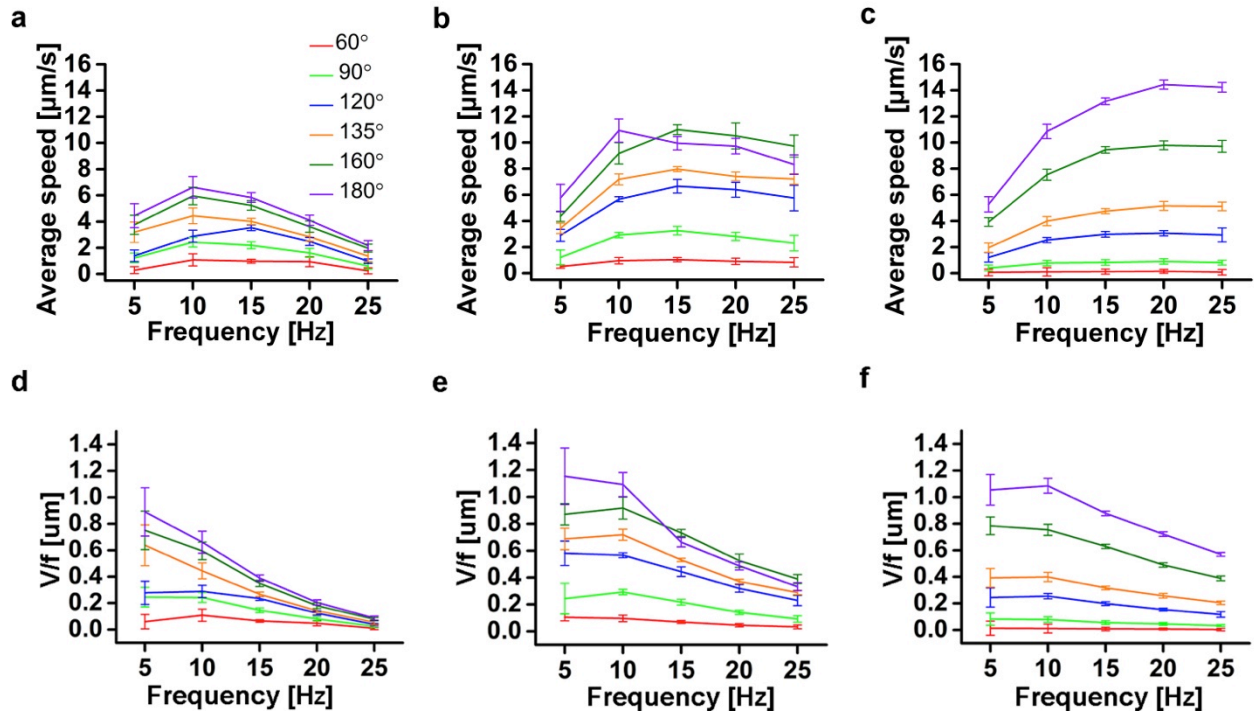

Figure 3. Average speed as a function of frequency (Hz) and angular sweep (2θ), and the net displacement per period $X = V/f$. (a),(b),(c) Average speed of a 1,2 and 3-link swimmers, respectively. (d),(e),(f) The net displacement per period $X = V/f$ of 1,2 and 3-link swimmers where V = speed and f = frequency. Swimmers were subjected to various field frequencies and angles ($B_A = 8.4$ mT). The angular sweep varies from $2\theta = 60°$ to $180°$ and the frequency varies from 5 Hz to 15 Hz with a step size of 5 Hz. The average speeds and standard deviation values were obtained from at least five speeds obtained from an image sequence.
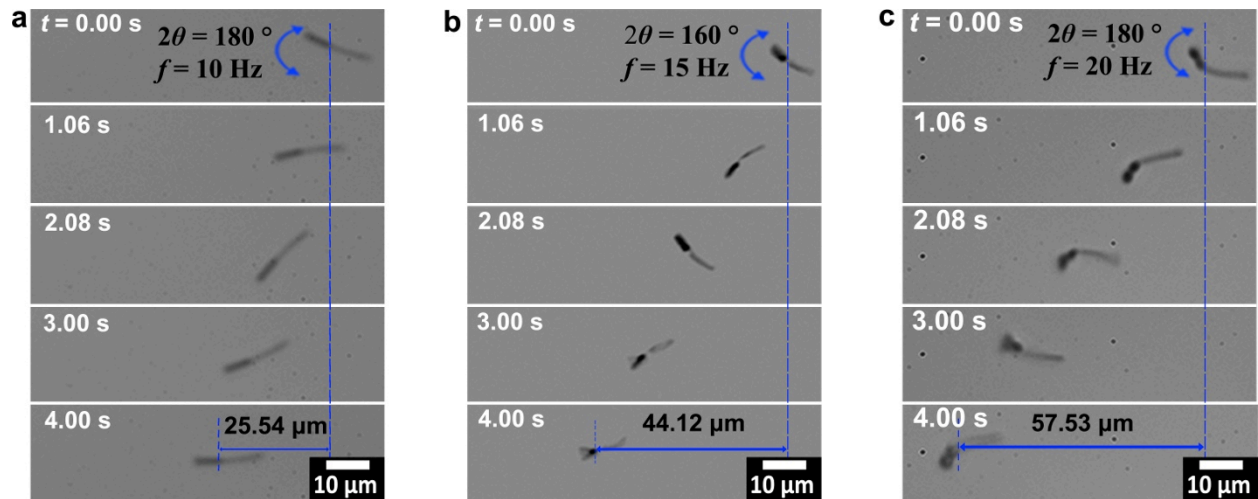
Figure 4. The propulsion of 1-, 2- and 3-link swimmers at the maximum speed. (a) The propulsion of 1-link swimmer with the maximum speed at $2\theta = 180°$ and $f = 10$ Hz (see SI Movie S4). (b) The propulsion of 2-link swimmer with the maximum speed at $2\theta = 160°$ and $f = 15$ Hz (see SI Movie S5). (c) The propulsion of 3-link swimmer with the maximum speed at $2\theta = 180°$ and $f = 20$ Hz (see SI Movie S6).